American Mineralogist, Volume 76, pages 1485–1501, 1991

Substitution of $^{[6,4]}$Al in phlogopite: Mica characterization, unit-cell variation, ^{27}Al and ^{29}Si MAS-NMR spectroscopy, and Al-Si distribution in the tetrahedral sheet

Susan Circone, Alexandra Navrotsky
Department of Geological and Geophysical Sciences, Princeton University, Princeton, New Jersey 08544, U.S.A.
R. James Kirkpatrick
Mineral Physics Program, Department of Geology, University of Illinois, 245 Natural History Building, 1301 West Green Street, Urbana, Illinois 61801, U.S.A.
Colin M. Graham
Department of Geology and Geophysics, University of Edinburgh, West Mains Road, Edinburgh EH9-3JW, United Kingdom

Abstract

The compositional and structural effects of the Tschermak's substitution $(^{[6]}Mg,^{[4]}Si)_{-1}(^{[6]}Al,^{[4]}Al)$ in phlogopite were investigated for nine synthetic magnesium aluminum phlogopite compositions. The observed synthetic mica compositions lie along the phlogopite-eastonite join, ranging between $0.00 \leq X_{east} \leq 0.92$, based on the formula $K(Mg_{3-x}Al_x)(Si_{3-x}Al_{1+x})O_{10}(OH)_2$, and extending well beyond the upper limit of $X_{east} = 0.62$ proposed by Hewitt and Wones (1975). High resolution ^{27}Al and ^{29}Si MAS-NMR spectra also indicate a continuous increase in the $^{[6,4]}$Al content of the micas. The $^{[4]}$Al/$^{[4]}$(Al + Si) ratios determined from electron microprobe analyses on fine-grained aggregates of the micas are in excellent agreement with the ^{29}Si NMR spectroscopic results. Thermogravimetric analyses indicate that the micas contain stoichiometric H_2O contents plus varying amounts of adsorbed H_2O. The onset of dehydroxylation is not significantly affected by increasing $^{[6,4]}$Al content.

Refinements of powder X-ray diffraction data indicate that the *a* and *b* unit-cell parameters decrease linearly with increasing $^{[6,4]}$Al content, corresponding to a 1.3% reduction in the lateral dimensions of the 2:1 layers from $X_{east} = 0.00$–0.92. The increasing misfit between adjacent tetrahedral and octahedral sheets is partially compensated by tetrahedral rotation. The calculated tetrahedral rotation angle increases linearly with increasing $^{[6,4]}$Al content, significantly decreasing the size of the interlayer cavity. The unit-cell volume decreases linearly with increasing $^{[6,4]}$Al content, and the volume of mixing is zero for the phlogopite-eastonite solid solution.

The extent of Al-Si ordering in the tetrahedral sheets of the synthetic micas has been determined by computer modeling of the ^{29}Si NMR spectra. The Al-Si distributions are short-range ordered, constrained primarily by the avoidance of adjacent Al tetrahedra. The computer simulations are further improved if the $^{[4]}$Al is distributed evenly throughout the sheet to minimize local charge imbalances. As the $^{[4]}$Al/$^{[4]}$(Al + Si) ratio increases from 0.24 to 0.47, the Al-Si distribution becomes increasingly ordered, converging with the long-range ordered distribution of strictly alternating Al and Si tetrahedra at high $^{[4]}$Al contents.

Introduction

The trioctahedral micas are stable over a wide range of pressure and temperature conditions and are important constituents of low- to high-grade metamorphic, intrusive, and extrusive igneous and upper mantle rocks. The chemical variation of natural biotite is approximately represented by two substitution mechanisms: $^{[6]}Mg^{2+} = {}^{[6]}Fe^{2+}$ and $^{[6]}Mg^{2+},{}^{[4]}Si^{4+} = {}^{[6,4]}Al^{3+}$. The Al content of biotite depends in part on the bulk-rock composition and the coexisting phases in the rock (Guidotti, 1984; Speer, 1984). In metamorphic biotite, the $^{[6]}$Al content is largely charge balanced by excess $^{[4]}$Al. The extent of $^{[6,4]}$Al substitution is limited to less than 0.40 excess $^{[4]}$Al per four tetrahedral sites in Fe-bearing biotite and decreases with increasing Mg/(Mg + Fe) content (Guidotti, 1984). Biotite of igneous origin has similar solid solution limits (Speer, 1984).

Previous phase equilibria studies of trioctahedral micas have focused on the end-members phlogopite, annite, their intermediate solid solutions, and iron-aluminum (Mg-free) biotite (e.g., Hewitt and Wones, 1984). Several experimental studies have examined the limits of Al substitution in trioctahedral micas. Crowley and Roy (1964) ob-

0003–004X/91/0910–1485$02.00

served decreases in the d values of the (005) and (060) reflections with increasing [6,4]Al content and proposed an upper limit of substitution of $K(Mg_2Al)(Al_2Si_2)O_{10}(OH)_2$, although they did not obtain 100% synthesis of mica for that bulk composition. Hewitt and Wones (1975) studied unit-cell variation in iron magnesium aluminum biotite and observed a linear decrease in unit-cell volume with increasing [6,4]Al content for the Fe-free micas. They proposed an upper limit of [6,4]Al substitution corresponding to $K(Mg_{2.38}Al_{0.62})(Al_{1.62}Si_{2.38})O_{10}(OH)_2$, based on the minimal size of a K^+-bearing interlayer site, which decreases in size as [4]Al increases. Robert (1976) studied the temperature dependence of [6,4]Al substitution in phlogopite, finding an upper limit of $K(Mg_{2.0}Al_{0.81}\square_{0.17})(Al_{1.46}Si_{2.54})O_{10}(OH)_2$, where $\square$ is an octahedral vacancy, at 600 °C and 1.0 kbar.

We have undertaken a two-part experimental study of synthetic magnesium aluminum phlogopite to investigate the structural changes and thermodynamic mixing properties of the Tschermak's substitution in phlogopite. The first part of the study, presented here, focuses on the characterization of the synthetic micas, the variation in unit-cell parameters, and the extent of Al-Si ordering with increasing [4]Al. The second part will focus on the thermodynamic mixing properties of the solid solution (Circone and Navrotsky, 1990).

The synthetic micas have been characterized using the following techniques: electron microprobe analysis, thermogravimetric analysis, powder X-ray diffraction, and ^{29}Si and ^{27}Al MAS-NMR spectroscopy. The ^{27}Al spectra of 2:1 layer silicates contain information on the coordination state of Al (Müller et al., 1981) and the relative proportion of [6]Al and [4]Al (Kinsey et al., 1985; Woessner, 1989). The ^{29}Si MAS-NMR spectra of 2:1 layer silicates contain information about the distribution of Al and Si in the tetrahedral sheets. The peaks in the ^{29}Si spectra arise from different next-nearest-neighbor (NNN) environments of the Si nuclei and can be resolved for Si on sites surrounded by 0, 1, 2, or 3 NNN Al atoms (e.g., Lippmaa et al., 1980; Sanz and Serratosa, 1984). The [4]Al/[4](Al + Si) ratio can be calculated from the observed intensities of the peaks (Sanz and Serratosa, 1984), providing a reliable alternative to other types of chemical analysis. Computer modeling of the ^{29}Si spectra also provides information about the degree of Al-Si ordering in the tetrahedral sheets (Herrero et al., 1985a, 1985b, 1987), which is an important factor in determining the thermodynamic properties of micas. Single crystal X-ray diffraction studies suggest that Al-Si ordering is uncommon in natural *1M* trioctahedral micas (Bailey, 1984). Previous modeling of the ^{29}Si NMR spectra has shown that the Al-Si distributions in the tetrahedral sheet of 2:1 layer silicates with [4]Al/[4](Al + Si) ratios ≤ 0.50 are best described by the model of homogeneous dispersion of charges proposed by Herrero et al. (1985a, 1985b, 1987). In this model, the Al-Si distribution is short-range ordered, governed by Al-O-Al avoidance and by the minimization of local charge imbalance arising from $^{[4]}(AlSi_{-1})$ substitution. For the synthetic micas in this study, which were synthesized at low temperatures and have [4]Al/[4](Al + Si) ratios approaching 0.5, the distribution of Al and Si and the extent of ordering must be determined to address properly the thermodynamic properties of magnesium aluminum phlogopite.

Sample preparation and experimental methods

Sample synthesis

Nine micas were synthesized hydrothermally across the join phlogopite $KMg_3(AlSi_3)O_{10}(OH)_2$–eastonite $K(Mg_2Al)(Al_2Si_2)O_{10}(OH)_2$. The starting materials were gels made following the method of Hamilton and Henderson (1968). The gel compositions were checked by X-ray fluorescence analysis (Table 1) and lie on the ideal anhydrous join (within ±0.7 wt% of the ideal weight percent content for all oxides), although SiO_2 is consistently high. The nominal gel compositions, denoted by X_{gel} and referenced to the chemical formula $K(Mg_{3-x}Al_x)(Si_{3-x}Al_{1+x})O_{10}(OH)_2$, are evenly spaced across the phlogopite-eastonite join at 0.125 mole fraction increments. The mica compositions will be denoted by X_{east} for the measured mole fraction of the Tschermak's substitution.

The micas were synthesized in an internally heated Ar gas pressure vessel in sealed Pt capsules from the gels and distilled H_2O (at least 9% by weight). A variety of P,T conditions were investigated to try to determine the optimal synthesis conditions to produce 100% mica products. The following observations (based on optical examination, powder X-ray diffraction, and electron microprobe analysis, described below) describe the synthesis products and are not phase equilibria results because the experiments were not reversed and their durations may not have been sufficient to achieve equilibrium.

Gels with $0.000 \leq X_{gel} \leq 0.375$ produced approximately 100% on-composition micas between 650 and 1000 °C at 2.0–5.0 kbar. The compositions of the micas synthesized at 1000 °C, 5.0 kbar were verified by microprobe analysis of grains 5 μm × 10 μm in size. Gels with $X_{gel} \geq 0.500$ produced multiphase products containing Mg,Si-rich micas and abundant $MgAl_2O_4$ spinel (± minor kalsilite and corundum) at 900 °C, 5.0 and 8.5 kbar and 1000 °C, 6.1 kbar. The compositions of the micas synthesized at 900 °C, 8.5 kbar ranged from $X_{east} = 0.46$ to 0.58 (determined by microprobe analysis). For these same starting compositions, experiments at 450 °C, 6.7 kbar and 650 °C, 6.7 kbar produced mica plus corundum. The amount of corundum was reduced by decreasing the synthesis temperature with increasing X_{gel} to a minimum of 400 °C. Pressure did not significantly affect the product assemblage. These observations are consistent with the results of Robert (1976), who found that the amount of [6,4]Al substitution in phlogopite decreased with increasing temperature between 600 and 1000 °C at 1.0 kbar. The most aluminous phlogopite reported by Robert (1976) was synthesized at 600 °C, 1.0 kbar and is compositionally similar to a synthetic mica in this study (from the gel with $X_{gel} = 0.500$). The synthetic magnesium aluminum phlogopite

TABLE 1. Synthesis conditions of the magnesium aluminum phlogopite samples and XRF analyses of gel starting materials

			Starting compositions (wt%)**			
X_{gel}	T (°C)*	Duration (h)	K_2O	MgO	Al_2O_3	SiO_2
0.000	650	93	11.50(−30)	29.83(−45)	12.65(−12)	45.83(68)
0.125	650	120	11.52(−27)	29.05(04)	16.00(05)	43.43(18)
0.250	650	116	11.54(−24)	27.41(−32)	19.03(−11)	41.82(48)
0.375	650	111	11.63(−15)	26.25(−21)	21.97(−34)	39.85(40)
0.500	650	116	11.56(−21)	25.06(−13)	25.38(−11)	37.84(29)
0.625	475	122	11.63(−14)	23.91(−01)	28.36(−30)	35.80(15)
0.750†	450	184	11.39(−37)	22.72(07)	31.78(05)	33.99(23)
0.875†	400	251	11.58(−18)	21.33(−05)	34.81(−18)	32.08(21)
1.000	400	427	11.07(−32)	20.37(26)	38.32(16)	29.97(−01)

* Uncertainties are ±10 °C. All samples synthesized at 5.0 ± 0.1 kbar.

** Values in parentheses represent the deviation of the gel composition from the ideal composition of the anhydrous mica. For example, 11.49(−31) signifies that the weight percent K_2O is 0.31 wt% less than the ideal composition.

† These samples were ground and rerun with excess H_2O at the same P,T conditions for 127 (X_{gel} = 0.750) and 189 (X_{gel} = 0.875) h to enhance crystallinity.

samples used in this study were synthesized at 5.0 kbar and the temperatures listed in Table 1.

Optical examination

The synthetic magnesium aluminum phlogopite samples are composed of coherent aggregates up to 150 μm across of finely crystallized mica platelets with submicrometer to 2-μm lateral dimensions. The micas synthesized at 650 °C also contain some acicular grains approximately 1 × 4 μm in size. Corundum was optically discernible in the Al-rich samples ($X_{gel} \geq 0.500$), occurring as sporadic patches in some aggregates. No other impurities are optically detectable.

Electron microprobe analysis

Chemical analyses of the synthetic magnesium aluminum phlogopite samples were obtained using the Cameca Camebax at Edinburgh University and the JEOL 8600 Superprobe at Rutgers University. Aggregates of mica were mounted in epoxy on glass slides, polished, and C coated. Their exposed surfaces were unavoidably uneven because of their multiparticulate nature. A 15 kV accelerating voltage and beam currents of 3.0–7.3 nA were used. X-ray intensities were measured by wavelength dispersive spectrometry. Absorption and fluorescence corrections were applied to the raw data (ZAF correction procedures on the Cameca data and Bence-Albee correction procedures on the JEOL data). The composition data exhibit no systematic differences on the basis of instrument, beam current, or correction procedure used.

The sum of the weight percent oxides determined in each analysis ranged from 68 to 95%, lower than expected (~95.7%) based on independently determined H_2O contents (see below). The low totals may result from reduced X-ray production in the excitation volume because of the void space within the aggregates and the uneven surfaces of the analyzed grains. The compositions of the micas (Table 2) have been normalized to sum to the expected total (100% − wt% H_2O). There is no correlation between the normalized compositions and the measured weight percent totals. For the normalized compositions, scatter about the mean is normally distributed, and the mean and median are always less than 0.4 wt% apart. The scatter is high relative to the precision obtainable on coarse-grained

TABLE 2. Electron microprobe analyses of synthetic magnesium aluminum phlogopite samples

X_{gel}:	0.000	0.125	0.250	0.375	0.500	0.625	0.750	0.875	1.000
X_{east}:	0.00	0.13	0.24	0.32	0.45	0.56	0.70	0.80	0.92
No. of analyses:	51	54	37	24	22	34	40	45	22
				Weight percent oxides*					
K_2O	10.68(07)	11.01(04)	10.19(16)	10.42(15)	10.41(12)	9.97(13)	10.76(10)	10.62(09)	10.84(16)
MgO	28.56(08)	27.51(07)	26.38(18)	25.57(17)	24.48(30)	23.14(22)	21.69(24)	20.71(20)	19.74(24)
Al_2O_3	12.08(17)	15.29(18)	18.24(49)	20.16(51)	23.29(69)	26.61(48)	29.53(50)	32.22(43)	34.65(62)
SiO_2	44.43(18)	41.87(16)	40.89(38)	39.41(41)	37.43(51)	36.33(43)	34.00(42)	32.60(34)	30.83(61)
Wt% total	95.75	95.68	95.70	95.56	95.61	96.05	95.98	96.15	96.06
				Cations per 11 O atoms					
Si	3.06	2.90	2.81	2.72	2.59	2.49	2.35	2.24	2.13
[4]Al	0.94	1.10	1.19	1.28	1.41	1.51	1.65	1.76	1.87
[6]Al	0.04	0.15	0.29	0.36	0.48	0.64	0.75	0.86	0.95
Mg	2.93	2.84	2.71	2.63	2.52	2.36	2.23	2.12	2.03
K	0.94	0.97	0.90	0.92	0.92	0.87	0.95	0.93	0.96
Sum	7.91	7.96	7.90	7.91	7.92	7.87	7.93	7.91	7.94

Note: Weight percent oxide compositions are normalized as described in text.

* Error in parentheses is two standard deviations of the mean of the number of analyses listed above. For example, 10.68(07) signifies 10.68 ± 0.07 wt%.

samples and is attributed to random physical variations on the scale of the interaction volume (grain boundaries and void space between individual platelets, uneven upper surface, presence of corundum in some aggregates).

The following observations support the validity and accuracy of the analyses in Table 2. The compositions of the micas are equivalent to the starting gel compositions less the amount of excess corundum in some synthesis products. The modal weight percent of corundum was calculated using the program LSMODES (after the method of Bryan et al., 1969) and the gel and mica compositions (in Tables 1 and 2, respectively). The calculated modal weight percent of corundum increases from 0.0 to 3.9 wt% as X_{gel} increases. The calculated stoichiometries are typical of trioctahedral micas and suggest that the octahedral sheets do not contain significant vacancies. Both the ^{27}Al and ^{29}Si NMR spectra reflect the compositional trends indicated by the microprobe data. Furthermore, the excellent agreement of tetrahedral $^{[4]}$Al/$^{[4]}$(Al + Si) ratios calculated from the ^{29}Si NMR spectra (discussed below) lend strong support to the microprobe analyses.

Thermogravimetric analysis (TG)

The H_2O contents of the synthetic magnesium aluminum phlogopite samples were measured using the electronic microbalance of a Setaram TG-DSC 111 and a custom built furnace capable of heating to 1150 °C. Analyses were made on 15–20 mg samples dried overnight at 110 °C. Two samples each of the four most Mg,Si-rich micas were scanned at 10 °C per min from 30 to 1130 °C (experiments A1 and A2 for each mica). One sample each of the five most Al-rich micas was scanned under the above conditions in one analysis (experiment A). Because these samples lost more weight below 730 °C than the Al-poor ones, a sample of each Al-rich mica was first scanned at 10 °C per min from 30–730 °C, then equilibrated isothermally for 6–21 min (experiment B). Each sample was cooled and later scanned at 10 °C per min from 30 to 1130 °C (experiment C) to determine the reversibility of the low-temperature weight loss. All TG analyses were made in air. The observed weight loss percentages were corrected for the presence of excess corundum (determined from the modal analyses described above). Measured weight losses are accurate to ±0.20 wt%.

Powder X-ray diffraction

All X-ray diffraction (XRD) measurements were made with a Scintag Pad V automated diffractometer equipped with a solid state detector. Samples of the micas were mixed with NaCl as an internal standard and mounted on a quartz crystal cut parallel to the (0001) plane. Scans were made at 0.2° 2θ per min using Cu$K\alpha$ radiation. The only detectable impurity phase in the samples is corundum, identified by a small peak at 43.3° 2θ corresponding to the (113) reflection.

The patterns contain peaks typical of a *1M* or *3T* synthetic phlogopitic mica. Peaks have been indexed assuming the *1M* polytype (*C*2/*m*). Relative peak intensities suggest that the mounts were approximately randomly oriented (Clemens et al., 1987). All patterns contain (*hkl*) reflections, ruling out the *1Md* polytype that has been observed previously in low-temperature synthetic phlogopite (Yoder and Eugster, 1954; Clemens et al., 1987).

Peak positions were corrected using the (111), (200), (220), (311), (222), (400), (420) reflections of NaCl (a = 5.6402 Å). The unit-cell parameters were calculated using a version of Appleman and Evans' (1973) least-squares refinement method. Refinements used 19–23 reflections: (111), ($\bar{1}$12), (003), (112), ($\bar{1}$13), (023), (130), ($\bar{1}$31)-(200), (004), (131), ($\bar{1}$32)-(201), ($\bar{2}$21), ($\bar{2}$03), (202)-($\bar{1}$33), (005), (203), ($\bar{2}$41), ($\bar{1}$35), (060), (061)-(330), ($\bar{2}$07)-(136), ($\bar{2}$61)-($\bar{4}$01), (260), (333). Peaks were double indexed only when the calculated d values for the (*hkl*) remained within 0.04° 2θ of one another across the join.

^{29}Si and ^{27}Al MAS-NMR

The NMR spectra were obtained with two "home built" pulse-Fourier transform NMR spectrometers at H_0 = 8.45 T (^{29}Si) and 11.7 T (^{27}Al) described previously by Smith et al. (1983) and Turner et al. (1986). Experimental conditions were as follows. At 8.45 T, corresponding to a ^{29}Si frequency of 71.5 MHz, samples were rotated at 3.3–4.9 kHz and the 45° pulse widths were 5 μs; at 11.7 T, corresponding to ^{27}Al frequency of 130.3 MHz, samples were rotated at 5.4 kHz and the 45° pulse widths were 1.8 μs. Chemical shifts are reported in ppm relative to external tetramethylsilane (TMS, ^{29}Si) and 1 M $AlCl_3$ solution (^{27}Al).

We obtained relative populations for the Si(nAl) (n = 0, 1, 2, 3) Si environments by fitting the ^{29}Si MAS-NMR spectra to a sum of Gaussian curves using program NMRFIT, which is based on a Levenburg-Marquardt minimization algorithm (Press et al., 1986). The program computes 1σ for the spectral y values from the noise regions above and below the NMR peaks, and it is used to scale the uncertainties of the fitted parameters. Uncertainties in the fitted intensities (square root of the corresponding elements of the final covariance matrix) were less than 0.007 absolute (total integral 1.0). For the spectra with low signal-to-noise ratio, especially those from samples with high eastonite contents, the peaks at −83, −86, and −90 ppm are not well defined, but we obtained reasonable fits by fixing the peak widths to correspond to the widths observed in spectra with lower eastonite contents (2.3–3.0 ppm FWHH). The uncertainties also include the range of values possible from varying the fixed peak widths plus the uncertainty in the fitted intensities (1σ). Allowing all the peak widths to vary for the samples with X_{east} = 0.80 and X_{east} = 0.92 results in fits for which the residual in the peak area is less than the noise at the edge of the spectrum, indicating the fit is underconstrained.

Synthetic mica compositions

Results

The structural formulae of the synthetic magnesium aluminum phlogopite samples were calculated from the

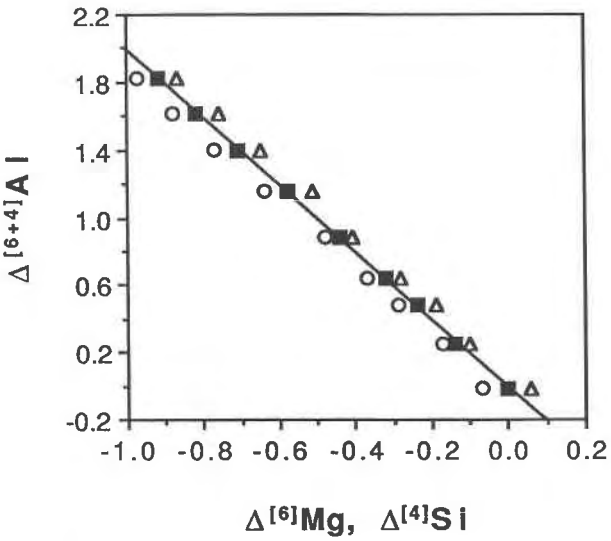

Fig. 1. Measured decreases in the number of Mg (circles) and Si (triangles) vs. increases in $^{[4+6]}Al$ based on the calculated structural formulae from microprobe analysis (Table 2) of the synthetic magnesium aluminum phlogopite samples. Changes in mica composition are calculated relative to the formula for pure phlogopite. A linear regression of the averaged changes in Mg and Si (squares) yields a slope of 2.00 ± 0.02 and a coefficient of determination r^2 of 1.00.

normalized weight percent oxide compositions on the basis of 11 O atoms (Table 2). Using the ideal phlogopite formula as the reference composition, the incremental decreases in $^{[6]}Mg^{2+}$ and $^{[4]}Si^{4+}$ and increases in $^{[6,4]}Al^{3+}$ can be calculated for each synthetic mica (Fig. 1). If the amount of Tschermak's substitution is defined as $x = 3.00 - {}^{[4]}Si$, the corresponding $^{[6]}Al$ contents are always ~0.1 higher than x (the distance between circles and triangles on Fig. 1), reflecting the small excess Si contents of the gels (Table 1). The excess $^{[6]}Al^{3+}$ component is approximately charge balanced by a deficiency of $^{[6]}Mg^{2+}$ and K^+ in the interlayer site. Nonetheless, if the incremental changes in octahedral and tetrahedral site compositions are averaged, the resulting correlation is a line with a slope corresponding to Tschermak's substitution (Fig. 1). These averaged values are the X_{east} listed in Table 2. The presence of excess corundum in the samples with $X_{east} \geq 0.24$ results in $X_{east} < X_{gel}$ for these samples.

The solid solution between phlogopite and eastonite appears to extend approximately to the eastonite endmember. The most Al-rich synthetic mica in this study has the composition $X_{east} = 0.92$, which is beyond the upper limit ($X_{east} \approx 0.62$) proposed by Hewitt and Wones (1975) for the phlogopite-eastonite join. This result is discussed in detail below.

Thermogravimetric analysis

Results

In general, the TG curves and the measured weight losses of the synthetic micas are typical of Fe-poor trioctahedral micas (e.g., Vedder and Wilkins, 1969). The weight loss curves of the synthetic magnesium aluminum phlogopite samples with $X_{east} = 0.24$ and 0.70 (Fig. 2) can be divided into two main regions: a low-temperature region (30–730 °C) showing minor weight loss and a high-temperature region (730–1130 °C) in which most of the weight loss occurs. We attribute the rapid weight loss above 730 °C to mica dehydroxylation. The expected weight percent change from the release of 1 mol of H_2O per mole of magnesium aluminum phlogopite is 4.3 wt%. Based on the observed weight losses above 730 °C (Table 3), the micas with $X_{east} \leq 0.45$ have stoichiometric H_2O contents

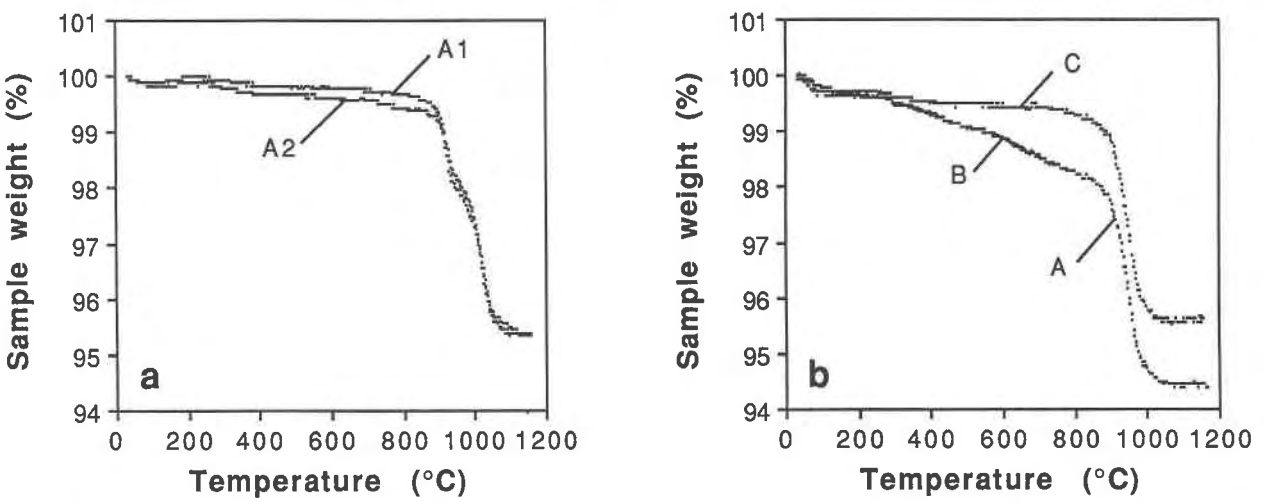

Fig. 2. Weight loss vs. temperature from thermogravimetric analysis of synthetic magnesium aluminum phlogopite samples. **(a)** Mica with $X_{east} = 0.24$; experiments A1 and A2 are continuous scans between 30 and 1130 °C. **(b)** Mica with $X_{east} = 0.70$; experiment A is a continuous scan between 30 and 1130 °C. Experiment B is a continuous scan between 30 and 730 °C. Experiment B was then cooled to 30 °C and rescanned between 30 and 1130 °C (experiment C). Differences in the weight loss patterns of experiments A and C illustrate the irreversible weight loss observed between 450 and 730 °C.

TABLE 3. Weight losses of synthetic magnesium aluminum phlogopite samples between 30 and 1130 °C

Mole fraction X_{east}	Weight loss (wt%) 30–450 °C	450–730 °C	730–1130 °C	Total (wt%) 30–1130 °C
0.00*	−0.33	−0.05	−4.25	−4.63
0.13*	−0.34	−0.05	−4.29	−4.68
0.24*	−0.24	−0.11	−4.28	−4.63
0.32*	−0.22	−0.14	−4.35	−4.71
0.45**	−0.36	−0.15	−4.34	−4.81
†	−0.16	0.00	−4.23	−4.39
0.56**	−0.99	−0.75	−3.97	−5.67
†	−0.48	−0.05	−3.74	−4.27
0.70**	−0.86	−0.72	−4.00	−5.55
†	−0.50	−0.06	−3.82	−4.37
0.80**	−1.21	−0.69	−3.74	−5.51
†	−0.70	−0.11	−3.67	−4.48
0.92**	−1.07	−0.80	−3.82	−5.67
†	−0.93	−0.06	−3.66	−4.65

Note: Weight losses are referenced to the sample weights at 30 °C.

* Data are the averaged results from experiments A1 and A2 (samples continuously scanned from 30 to 1130 °C).

** Data for 30–450 °C and 450–730 °C are averaged results from experiments A and B (samples continuously scanned from 30 to 730 °C). Data for 730–1130 °C and for 30–1130 °C are the results from experiment A.

† Data are the results from experiment C (samples from experiment B continuously scanned from 30 to 1130 °C).

and the micas with $X_{east} > 0.45$ have slightly low H_2O contents but lose more weight between 450 and 730 °C. We attribute the weight losses between 30 and 450 °C to the release of adsorbed H_2O from the samples.

Powder XRD patterns of the dehydration products heated to 1130 °C show that the (001) mica reflections are present but greatly reduced in intensity and that no other mica peaks are detected. The remaining XRD peaks can be assigned to poorly crystallized forsterite and kalsilite. We conclude that dehydration is complete by 1130 °C. The persistence of the (001) reflection may suggest the presence of some dehydroxylated mica.

Discussion

The results for the thermogravimetric analysis were also used in planning the high-temperature solution calorimetry study at 704 °C on the magnesium aluminum phlogopite samples (Circone and Navrotsky, 1990). Based on differences in total weight loss and in the temperature distribution of that weight loss, the micas fall into two compositional groups, one with $X_{east} \leq 0.45$ and one with $X_{east} > 0.45$ (represented by Figs. 2a and 2b, respectively). Above 730 °C, the micas with $X_{east} \leq 0.45$ lose weight rapidly, the rate of weight loss reaching a local minimum near 940 °C (Fig. 2a). This episodic weight loss pattern may be related to slight energetic differences in the −OH, with −OH bonded to [6]Al lost in the lower temperature episode. This interpretation is supported by vibrational studies of trioctahedral micas, which show that the −OH stretching frequency of OH bonded to $2Mg^{2+}Al^{3+}$ in the octahedral sheet is lower than that of OH bonded to $3Mg^{2+}$ (Vedder and Wilkins, 1969), indicating that the [6](Mg$_{-1}$Al) substitution weakens the O-H bond.

The micas with $X_{east} > 0.45$ do not have an episodic weight loss pattern above 730 °C (Fig. 2b), but the onset of rapid dehydroxylation occurs ~20–30 °C lower than for micas with $X_{east} \leq 0.45$. Furthermore, between 450 and 730 °C these micas irreversibly lose 0.7–0.8% of their weight (compare experiments A and B with C, Fig. 2b and Table 3), whereas the weights of the samples with $X_{east} \leq 0.45$ decrease less than 0.1%. This irreversible weight loss between 450 and 730 °C may arise from early loss of −OH associated with higher [6]Al contents of these micas and would explain the low weight losses observed between 730 and 1130 °C (compare experiments A and C in Fig. 2b and Table 3). Alternatively, the weight loss could arise from loss of −OH near octahedral vacancies that occurs between 500 and 800 °C (Vedder and Wilkins, 1969). However, this explanation is unlikely for the synthetic micas in this study, which have negligible octahedral vacancies (<0.03 per three octahedral sites, Table 2). If the weight losses between 450 and 730 °C (measured in experiments A and B) are included in the H_2O contents of the micas with $X_{east} > 0.45$, then these micas contain between 4.4 and 4.7 wt% H_2O, slightly higher than the ideal H_2O contents.

UNIT-CELL PARAMETERS AND VARIATION

Results

The substitution of [6,4]Al into phlogopite has a marked effect on the unit-cell parameters *a, b, c,* and β. The values for the phlogopite end-member ($X_{east} = 0.00$, Table 4) are similar to previously published values for synthetic phlogopite (Yoder and Eugster, 1954; Hewitt and Wones, 1975). With increasing [6,4]Al content, *a* and *b* decrease linearly, but *c* and β decrease to a minimum at $X_{east} = 0.56$ and then increase (Table 4, Fig. 3). In other studies of synthetic magnesium aluminum phlogopite, Hewitt and Wones (1975) observed similar trends in the unit-cell parameters and Crowley and Roy (1964) observed decreases in the *d* values of the (060) and (005) reflections. The net effect of these changes in the unit-cell parameters is an approximately linear reduction in unit-cell volume. The results for linear regressions of X_{east} vs. *a, b* and unit-cell volume are in Table 5. A linear regression of the synthetic magnesium aluminum phlogopite unit-cell volume data of Hewitt and Wones (1975) is almost identical to the results in this study (Table 5). The smaller slope obtained from their data may be tied to the overestimation of the [6,4]Al contents of their samples. The compositions of two of their samples, with expected compositions of $X_{east} = 0.50$ and 0.62, were measured using analytical TEM (Livi and Veblen, 1987) and determined to be $X_{east} = 0.38$ and 0.50, respectively. These discrepancies between nominal and observed [6,4]Al contents are higher than those in this study (Table 2) and probably result from the higher synthesis temperatures (700–850 °C) used in their study.

The deviation of sample $X_{east} = 0.56$ from the ideal volume of mixing line reflects its relatively small measured *c* cell parameter (Fig. 3). The quality of the refinement is questionable because the powder XRD pattern

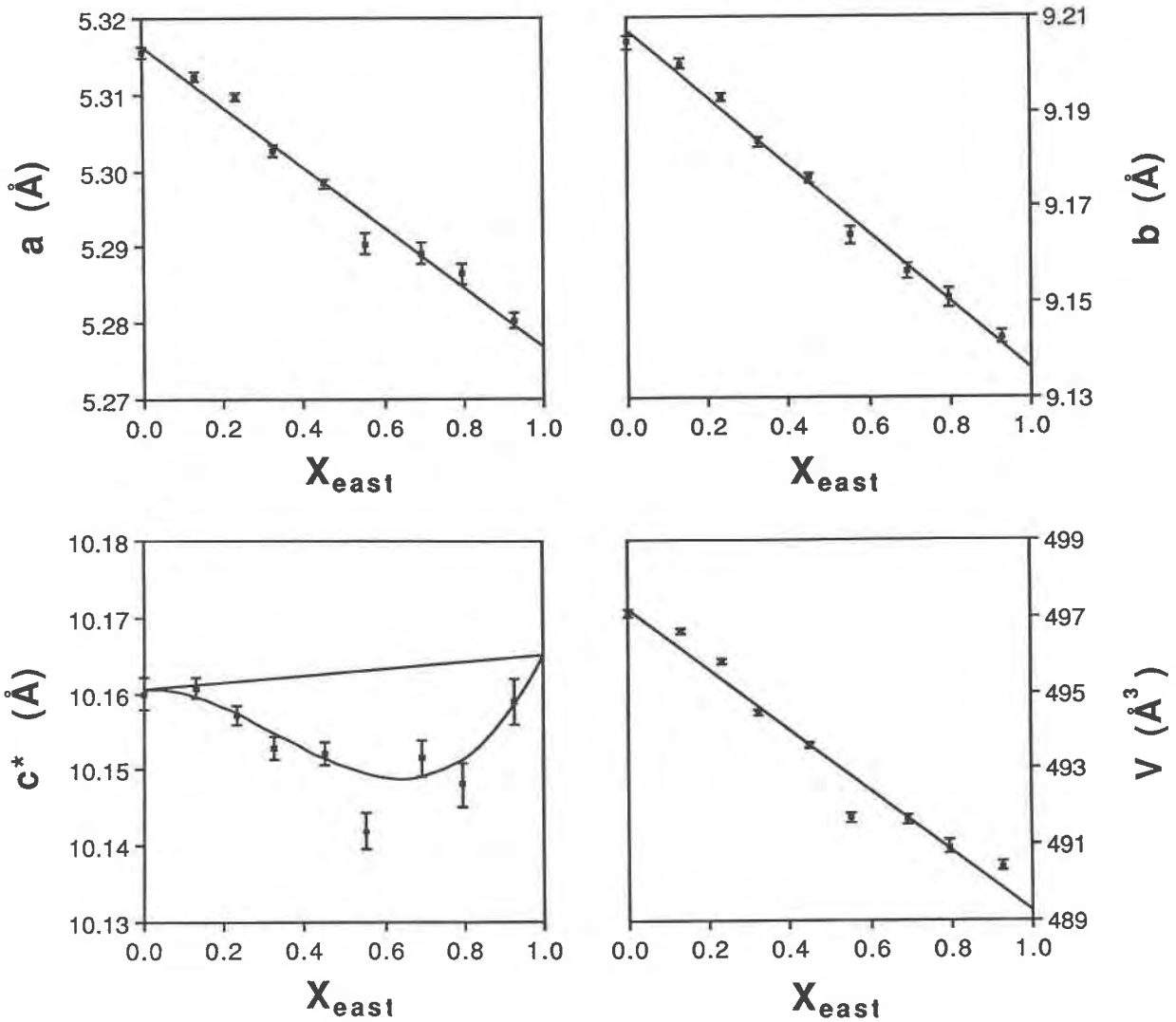

Fig. 3. Unit-cell parameters of the synthetic magnesium aluminum phlogopite samples vs. the measured mole fraction X_{east} of Tschermak's substitution. The parameter c^*, the repeat distance of 2:1 layers perpendicular to the a-b plane, is defined as $c^* = c \cos(\beta - 90°)$. Brackets represent the uncertainties listed in Table 3.

had poorer peak resolution than those of the other micas and peak positions were difficult to measure. We suspect that this mica is poorly crystallized because it was synthesized at low temperature for a relatively short duration (Table 1).

Discussion

The observed changes in the unit-cell dimensions directly reflect the changes in mica composition. The a and b unit-cell parameters are oriented in the plane of the 2:1

TABLE 4. Unit-cell parameters of synthetic magnesium aluminum phlogopite samples

X_{east}	a (Å)	b (Å)	c (Å)	β (°)	V (Å^3)	α_{calc} (°)
0.00	5.3154(08)	9.2046(13)	10.3136(17)	99.90(02)	497.09(11)	9.2
0.13	5.3123(06)	9.2001(09)	10.3134(12)	99.87(01)	496.60(07)	10.4
0.24	5.3097(06)	9.1931(09)	10.3100(11)	99.88(01)	495.79(07)	11.2
0.32	5.3027(08)	9.1838(10)	10.3057(13)	99.88(01)	494.43(08)	11.9
0.45	5.2983(06)	9.1762(10)	10.3046(13)	99.87(01)	493.59(08)	12.8
0.56	5.2904(14)	9.1640(17)	10.2936(21)	99.85(02)	491.70(13)	13.6
0.70	5.2892(13)	9.1567(16)	10.3048(20)	99.90(02)	491.65(13)	14.4
0.80	5.2865(13)	9.1510(21)	10.3017(25)	99.91(02)	490.93(16)	15.0
0.92	5.2803(10)	9.1426(14)	10.3132(26)	99.92(02)	490.43(14)	15.7

Note: Numbers in parentheses are standard error estimates in last significant figures.

TABLE 5. Coefficients and constants for linear regression correlations of mole fraction X_{east} vs. structural parameters

Structural parameter	Intercept	Slope	r^2
a (Å)	5.316(1)	−0.040(2)	0.988
b (Å)	9.207(1)	−0.071(3)	0.996
V (Å^3)	497.20(33)	−7.94(60)	0.981
V (Å^3)*	497.01(11)	−7.49(30)	0.997
V (cm^3/mol)	149.71(10)	−2.39(18)	0.981
α (°)	9.5(1)	7.0(2)	0.997

Note: Equation form is $y = mx + b$, where x is the observed mole fraction of Tschermak's substitution (X_{east}). Numbers in parentheses are standard error estimates of m and b in last decimal places quoted.
* Results from Hewitt and Wones (1975).

layers and describe the lateral dimensions of the joined octahedral and tetrahedral sheets. The inwardly pointing apical O atoms of the two tetrahedral sheets and the OH anions form the coordination polyhedra for the octahedral cations. The 2:1 layer structure requires that the sheets have similar lateral dimensions, but for most micas the octahedral sheet is smaller than the tetrahedral sheet (Bailey, 1984). The misfit between sheets can be compensated by thinning or thickening of appropriate sheets and by counterrotation of adjacent tetrahedra within the plane of the sheet (Bailey, 1984). The tetrahedral rotation can be estimated using the equation (Radoslovich, 1961)

$$\alpha = \cos^{-1}\left(\frac{b_{observed}}{b_{ideal}}\right) \quad (1)$$

where α (in degrees) is the rotation of the tetrahedra from ideal hexagonal symmetry and b_{ideal} is estimated using the equation

$$b_{ideal}\ (\text{Å}) = 9.15 + 0.74y \quad (2)$$

where y is the $^{[4]}Al/^{[4]}(Al + Si)$ ratio (Bailey, 1984). In phlogopite, the observed b cell dimension (b = 9.205 Å, Table 4) is smaller than the calculated ideal dimension of the $AlSi_3O_{10}$ tetrahedral layers (b_{ideal} = 9.3239 Å), resulting in a tetrahedral rotation angle of $\alpha = \cos^{-1}(9.2046\ \text{Å}/9.3239\ \text{Å}) = 9.2°$.

In the synthetic magnesium aluminum phlogopite samples, the Tschermak's substitution involves cation exchanges in both sheets. In the tetrahedral sheet, the replacement of Si^{4+} by Al^{3+}, with ionic radii of 0.26 Å and 0.39 Å, respectively (fourfold coordination, Shannon and Prewitt, 1969), should increase the average size of a tetrahedron and increase the lateral dimensions of these sheets (Eq. 2). However, in the octahedral sheet, replacement of Mg^{2+} by Al^{3+}, with ionic radii of 0.72 Å and 0.53 Å, respectively (sixfold coordination, Shannon and Prewitt, 1969), decreases the average size of an octahedron and the lateral dimensions of this sheet. Thus, increasing the $^{[6,4]}Al$ content of phlogopite must (1) decrease the lateral dimensions of the octahedral sheet, (2) increase tetrahedral rotation to compensate for the shrinking dimensions of the octahedral sheet, and (3) decrease the a and b unit-cell parameters. These predictions are confirmed by the results in Tables 4 and 5 and Figure 3.

Three of the magnesium aluminum phlogopite samples in this study have higher Al contents (X_{east} = 0.70, 0.80, and 0.92) than the limit of X_{east} = 0.62 proposed by Hewitt and Wones (1975). They suggested that the maximum $^{[4]}Al$ content in trioctahedral micas is limited by the minimum size needed for the interlayer cavity for a given interlayer cation. According to their argument, the size of the interlayer cavity decreases and the interlayer cation-O bond length decreases below a stable minimum length (~2.77 Å for K-O) as the tetrahedral rotation angle exceeds 14.7°.

Their substitution limit is based on a minimum stable K-O bond length, calculated using the following parameters for their synthetic mica with X_{east} = 0.62: M-O bond length of 2.02 Å, an $^{[4]}Al$ fraction of 0.41, a T-O bond length of 1.675 Å, and calculated tetrahedral rotation angle of 14.7°. However, analytical TEM analyses of this sample suggest that the $^{[4]}Al$ fraction is only 0.37 (Livi and Veblen, 1987). This lower $^{[4]}Al$ fraction would cause a decrease in the average T-O bond length, a decrease in the tetrahedral rotation angle, and an increase in the K-O bond length for a constant observed b cell dimension. Furthermore, a comparison of tetrahedral rotation angles obtained from structure refinements vs. those calculated using Equations 1 and 2 suggests that the calculated angles often overestimate the actual rotation angle by 2–3° (e.g., Table 3 of Weiss et al., 1987). Therefore, even the most aluminous sample in this study could have an actual tetrahedral rotation angle nearer to 13° and below the calculated limit of 14.7°. We conclude that the upper limit of $^{[6,4]}Al$ substitution proposed by Hewitt and Wones (1975) may be accurate in terms of the limiting structural parameters but allows for higher $^{[6,4]}Al$ contents.

The distances between the interlayer cation and the coordinating basal O atoms of the tetrahedral sheet, which decrease with increasing tetrahedral rotation, can increase if the interlayer cation props apart the 2:1 layers. Radoslovich and Norrish (1962) observed this in K-rich dioctahedral micas, where the K is too large for the interlayer cavity if full tetrahedral rotation has occurred. Evidence for this is present in the unit-cell data of the synthetic magnesium aluminum phlogopite samples. The interlayer distance between 2:1 layers decreases slightly (<0.02 Å) as X_{east} increases to 0.56 (c^* plot, Fig. 3) and is presumably related to octahedral thinning. But as X_{east} and the tetrahedral rotation increases further, the interlayer cavity becomes too small, the K cation props apart the 2:1 layer units, and c^* increases ~0.02Å from X_{east} = 0.56 to 0.92.

^{29}Si AND ^{27}Al MAS-NMR SPECTROSCOPY

Results

The peaks in the ^{29}Si MAS-NMR spectra of the synthetic magnesium aluminum phlogopite samples (Fig. 4) show systematic variation in intensity and are readily assigned to $Q^3(n\text{Al})$ sites in trioctahedral 2:1 layer silicates, where Q^3 signifies that there are three bridging O atoms per tetrahedron and n (n = 0, 1, 2, 3) is the number of

next-nearest-neighbor (NNN) tetrahedral Al atoms. For phlogopite ($X_{east} = 0.00$), the resonances at −90.7, −87.0, and −83.2 ppm correspond to Si with 0, 1, and 2 NNN Al, respectively. There are resonances at similar chemical shifts in the spectra of all the synthetic micas except for the mica with $X_{east} = 0.92$, in which $Q^3(0Al)$ is not discernible. In addition, a resonance at approximately −80 ppm corresponding to $Q^3(3Al)$ appears in the spectrum of the mica with $X_{east} = 0.13$ (not shown) and increases in intensity with increasing X_{east}. The chemical shifts do not change dramatically with changing composition, but the relative peak intensities of the $Q^3(nAl)$ sites vary systematically with increasing X_{east} (Table 6). We have ruled out the presence of unreacted gel starting material based on the absence of a broad peak near −110 ppm for amorphous silica gel (e.g., Brinker et al. 1988).

The ^{29}Si chemical shifts for the Q^3(0,1, and 2Al) sites are similar to those of a natural phlogopite sample (e.g., Sanz and Serratosa, 1984). The observed shifts in this study are less shielded (less negative) by ~3 ppm than those of various trioctahedral clays (Lipsicas et al., 1984; Weiss et al., 1987) and are less shielded by ~2 ppm than those of fluorophlogopite (Kinsey et al., 1985; Weiss et al., 1987). The $Q^3(3Al)$ peaks are 3 ppm more negative (more shielded) than that observed for a synthetic Mg-trioctahedral mica with an $^{[4]}Al/^{[4]}(Al + Si)$ ratio of 0.43 studied by Herrero et al. (1987). These discrepancies may arise from differences in octahedral sheet and interlayer site composition. The $Q^3(3Al)$ peaks are 3–4 ppm more negative than the corresponding $Q^3(3Al)$ peak of margarite (Mägi et al., 1984; Kinsey et al., 1985), but this difference probably results from the dioctahedral nature of margarite.

The spectra of samples with $X_{east} = 0.00$ and 0.13 also exhibit a small shoulder (<5% relative intensity) at −93.9 ppm. This shoulder probably corresponds to $Q^3(0Al)$ sites adjacent to K-deficient interlayer cavities, most likely in smectite-like layers. It is unlikely that it results from a framework aluminosilicate because no phase like this is detectable optically, by XRD or in the ^{29}Si NMR spectra, in which the chemical shifts of Q^4 sites are typically more negative than −105 ppm (Lippmaa et al., 1980; Mägi et al., 1984). Trioctahedral K-deficient clays, such as the saponite studied by Weiss et al. (1987), do yield chemical shifts near −94 ppm. The shoulder is not apparent in the spectra of the other synthetic magnesium aluminum phlogopite samples that are comparably K deficient (Table 2).

The ^{27}Al MAS-NMR spectra of the synthetic magnesium aluminum phlogopite samples (Fig. 5) contain resonances at approximately 65–70 ppm and 0–10 ppm, consistent with previously reported values for $^{[4]}Al$ and $^{[6]}Al$, respectively (Müller et al., 1981; Lipsicas et al., 1984; Kinsey et al., 1985). The broad resonance at 3 ppm is attributed to $^{[6]}Al$ in the mica, and the narrow band at 8 ppm is attributed to $^{[6]}Al$ in corundum, which is present in the samples with $X_{east} \geq 0.13$ but is optically discernible only in the samples with $X_{east} \geq 0.45$. The ^{27}Al peak maximum of $^{[4]}Al$ becomes more positive (from +65.0 to +70.5

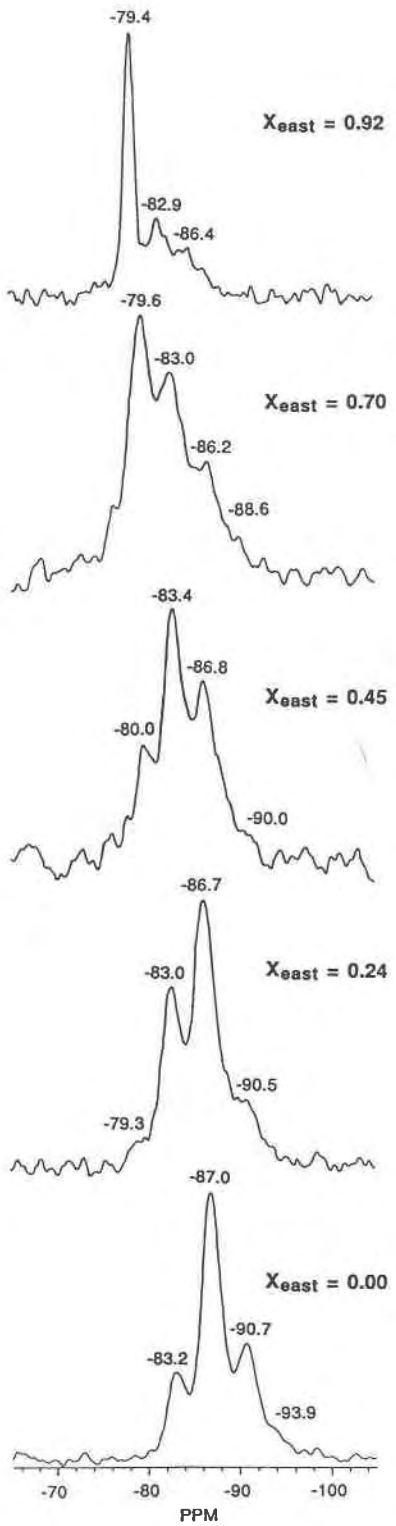

Fig. 4. The ^{29}Si MAS-NMR spectra of synthetic magnesium aluminum phlogopite samples. The resonances at approximately −90, −87, −83, and −80 ppm correspond to $Q^3(0Al)$, $Q^3(1Al)$, $Q^3(2Al)$, and $Q^3(3Al)$ sites in the mica, respectively. The spectra of micas with $X_{east} = 0.00$ and 0.13 (not shown) have a small shoulder at −94 ppm because of some K-deficient clay-like layers in these micas.

TABLE 6. Observed peak intensities of $Q^3(n\text{Al})$ components of the ^{29}Si NMR spectra, calculated $^{[4]}$Al/$^{[4]}$(Al + Si) ratios, and $^{[4]}$Al/($^{[4]}$Al + $^{[6]}$Al) ratios from ^{29}Si and ^{27}Al MAS-NMR spectroscopy and electron microprobe (probe) analysis

Mole fraction X_{east}	Intensities of $Q^3(n\text{Al})$*				$^{[4]}$Al/$^{[4]}$(Al + Si)		$^{[4]}$Al/($^{[4]}$Al + $^{[6]}$Al)	
	0Al	1Al	2Al	3Al	Probe	^{29}Si	Probe	^{27}Al
0.00	23.7(2.0)	56.7(1.0)	19.6(1.0)	—	0.235	0.242	0.959	0.971
0.13	19.8(2.0)	54.8(2.0)	22.9(1.0)	2.5(1.0)	0.275	0.265	0.880	0.943
0.24	12.3(2.0)	50.0(2.0)	33.2(1.0)	4.5(1.0)	0.298	0.302	0.804	0.909
0.32	10.5(2.0)	41.1(2.0)	40.7(2.0)	7.7(1.0)	0.320	0.327	0.780	0.859
0.45	7.8(2.0)	32.0(2.0)	44.1(1.0)	16.2(1.0)	0.352	0.360	0.746	0.832
0.56	8.9(2.0)	29.2(1.5)	37.6(1.0)	24.2(1.0)	0.378	0.371	0.702	0.761
0.70	4.2(2.0)	17.4(2.0)	33.5(2.0)	44.9(2.0)	0.412	0.422	0.688	0.719
0.80	6.0(2.0)	12.0(2.0)	28.5(3.0)	53.5(3.0)	0.440	0.433	0.672	0.692
0.92	1.0(1.0)	17.6(2.0)	27.1(3.0)	54.3(3.0)	0.468	0.439	0.663	0.664

* Intensities are normalized to 100%. Numbers in parentheses are uncertainties in intensities (see text).

ppm), and the peak width measured at half height decreases (from ~10 ppm to 4 ppm) with increasing $^{[4]}$Al content. The other peaks are spinning sidebands associated with the $^{[4]}$Al resonance.

The spectrum of pure phlogopite should exhibit only a single resonance corresponding to $^{[4]}$Al, but the broad, low-intensity resonance between 0 and 10 ppm indicates the presence of minor $^{[6]}$Al in the mica, which is also indicated by the calculated structural formula with 0.04 $^{[6]}$Al per three octahedral sites (Table 2). The intensity of the $^{[6]}$Al-corundum resonance increases as the bulk Al content of the starting gel increases, in agreement with observations from optical examination and the calculated modal weight percentages of corundum described previously.

Discussion

Both the ^{27}Al and ^{29}Si MAS-NMR spectra reflect the increasing Al content of the octahedral and tetrahedral sheets. In the ^{29}Si spectra, the changing relative peak intensities for the $Q^3(n\text{Al})$ sites indicate that the $^{[4]}$Al content of the tetrahedral sheets increases with increasing X_{east} (Table 6, Fig. 6). The composition of the tetrahedral sheet can be calculated using the expression (Sanz and Serratosa, 1984)

$$\frac{^{[4]}\text{Al}}{^{[4]}\text{Si}} = \frac{\frac{1}{3}\sum_{n=0}^{3} nI_n}{\sum_{n=0}^{3} I_n} \quad (3)$$

where I_n is the relative intensities of the $Q^3(n\text{Al})$ components of the spectra. This expression assumes that there are no $^{[4]}$Al-O-$^{[4]}$Al linkages (hereafter designated Al-O-Al) in the sheet, i.e., that only $[SiO_4]^{-4}$ tetrahedra are adjacent to $[AlO_4]^{-5}$ tetrahedra. This concept, first stated by Loewenstein (1954), appears to hold true for 2:1 layer silicates with $^{[4]}$Al/$^{[4]}$(Al + Si) $\leq$ 0.5. Several ^{29}Si NMR spectroscopy studies on natural and synthetic 2:1 layer silicates (Sanz and Serratosa, 1984; Lipsicas et al., 1984; Barron et al., 1985) have found close agreement between $^{[4]}$Al contents calculated from ^{29}Si spectra and those independently determined by chemical analysis.

The $^{[4]}$Al/$^{[4]}$(Al + Si) ratios for the synthetic magnesium aluminum phlogopite samples obtained from ^{29}Si NMR spectroscopy and from microprobe analysis are in excellent agreement (Table 6), consistent with the conclusion that the microprobe analyses accurately represent the synthetic mica compositions. These results are even consistent in finer detail. For example, in the spectrum of the mica with X_{east} = 0.00, the intensities of the Q^3(0Al) and Q^3(2Al) sites should be equal if the $^{[4]}$Al/$^{[4]}$(Al + Si) ratio is exactly 0.25 (Kinsey et al., 1985). However, the observed intensity of the Q^3(0Al) sites is greater than that of the Q^3(2Al) sites and the calculated $^{[4]}$Al/$^{[4]}$(Al + Si) ratio is 0.24, in agreement with the microprobe analysis for this mica. The result for the mica with X_{east} = 0.92 shows the largest discrepancy between microprobe analysis and NMR results and is discussed below.

The changing relative intensities of the $^{[4]}$Al and $^{[6]}$Al resonances in the ^{27}Al NMR spectra indicate that the $^{[6]}$Al content also increases with increasing Tschermak's substitution, but the agreement between the $^{[4]}$Al/($^{[4]}$Al + $^{[6]}$Al) ratios determined from the ^{27}Al spectra and from microprobe analysis is poorer than expected (within 0.05 of each other; Table 6 and Fig. 7). The differences in the $^{[4]}$Al/($^{[4]}$Al + $^{[6]}$Al) ratio are least at the phlogopite (almost no $^{[6]}$Al) and eastonite ends and greatest (~0.10) in the middle. Because the $^{[4]}$Al/$^{[4]}$(Al + Si) ratios determined by ^{29}Si NMR and microprobe analysis are in excellent agreement, we believe that the systematic overestimation of the $^{[4]}$Al/($^{[4]}$Al + $^{[6]}$Al) ratios from ^{27}Al NMR most likely results from some difficulty with the ^{27}Al NMR spectra. Such difficulties can arise because of signal loss during the instrumental dead time period at the beginning of data acquisition (e.g., Dupree et al., 1988). More signal is lost for broad peaks than for narrow ones. For quadrupole nuclides such as ^{27}Al, differences in peak breadth can result from a range of sites with different isotopic chemical shifts and overlapping peaks because of differences in second order quadrupole broadening, which arise from differences in electric field gradients at the nuclei. The pulse width of 1.8 μs could also contribute to the discrepancies in the $^{[4]}$Al/($^{[4]}$Al + $^{[6]}$Al) ratios. For the spectra in this study, there may also be a problem with correctly fitting the $^{[6]}$Al peak of corundum and mica and the overlapping spinning side band near −10 ppm (Fig. 5).

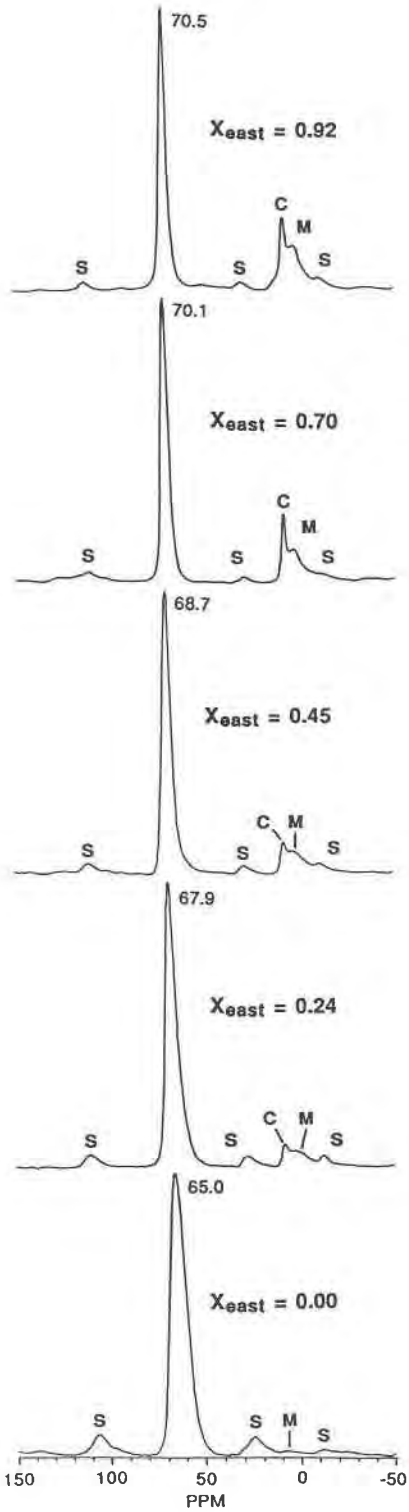

Fig. 5. The ^{27}Al MAS-NMR spectra of synthetic magnesium aluminum phlogopite samples. The resonances with peak maxima between ~70 and 65 ppm are [4]Al, and the resonances at ~0–10 ppm are [6]Al in the mica (labeled M). The narrow resonances labeled C at ~8 ppm are corundum. The spinning side bands are labeled S.

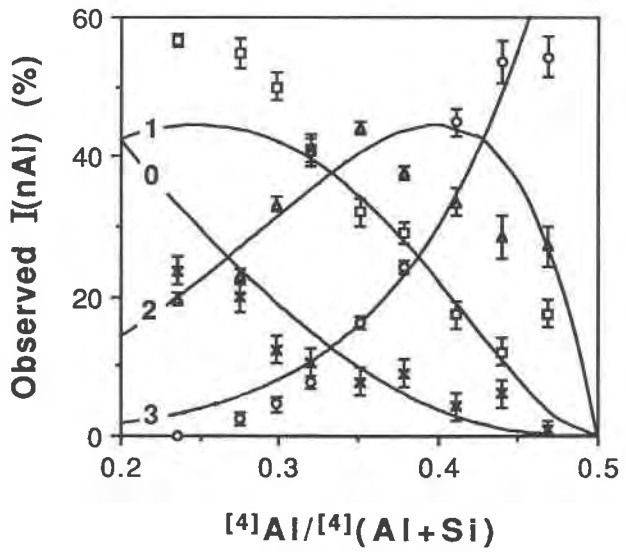

Fig. 6. Relative peak intensities of the $Q^3(n\text{Al})$ sites, where $n = 0$ (crosses), 1 (squares), 2 (triangles), and 3 (circles), in the ^{29}Si MAS-NMR spectra vs. the [4]Al/[4](Al + Si) ratio calculated from the microprobe analyses. The curves labeled 0, 1, 2, and 3 are the calculated intensities of the $Q^3(n\text{Al})$ sites, assuming the avoidance of [4]Al-O-[4]Al linkages (see description of AA model in the experimental methods section describing the computer modeling). Brackets represent the uncertainties listed in Table 6.

The decreasing width of the [4]Al peak with increasing [6,4]Al content could result from a decrease in its quadrupole coupling constant, from the range of [4]Al sites present, or from a combination of both. Quadrupole coupling constants decrease as the local [4]Al environment becomes

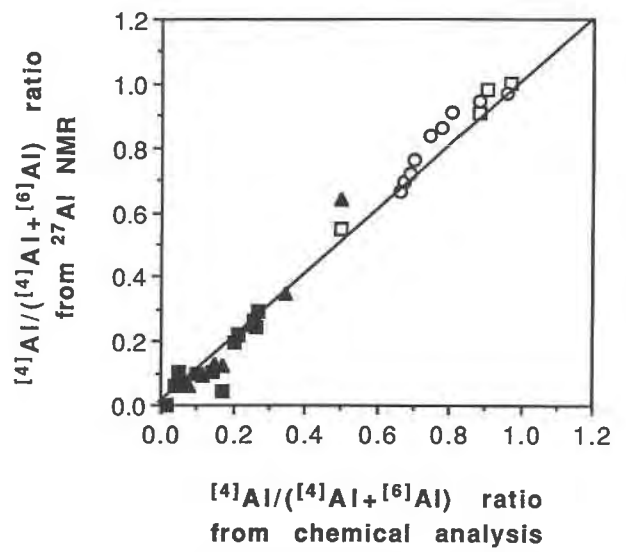

Fig. 7. The [4]Al/([4]Al + [6]Al) ratios of the synthetic magnesium aluminum phlogopite samples (circles) from microprobe analyses vs. ^{27}Al NMR. The results for various dioctahedral (closed symbols) and trioctahedral (open symbols) 2:1 layer silicates from Kinsey et al. (1985) (triangles) and Woessner (1989) (squares) are included for comparison.

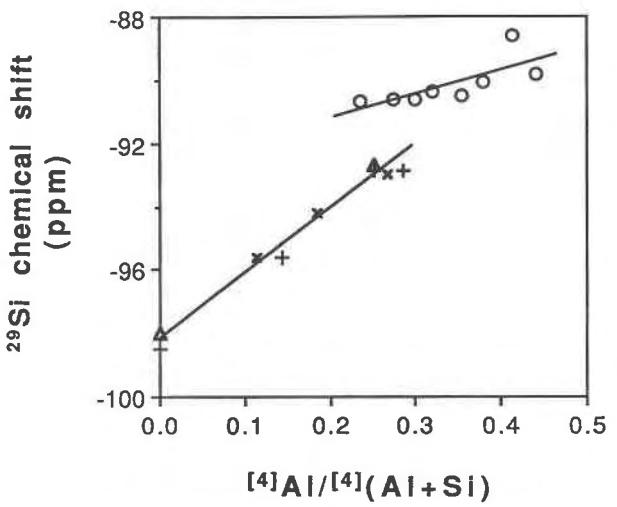

Fig. 8. The ^{29}Si chemical shift of the Q^3(0Al) resonances vs. $^{[4]}$Al/$^{[4]}$(Al + Si) ratio calculated from microprobe analysis (circles). Results from Lipsicas et al. (1984) (crosses), Kinsey et al. (1985) (triangles), and Weiss et al. (1987) (plusses) for various trioctahedral 2:1 layer silicates are included for comparison.

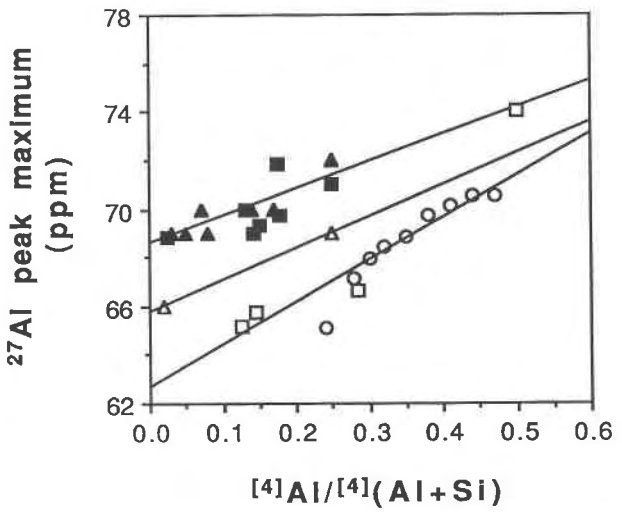

Fig. 9. The ^{27}Al peak maxima of $^{[4]}$Al vs. $^{[4]}$Al/$^{[4]}$(Al + Si) ratio calculated from microprobe analysis (open circles, this study). The results for various dioctahedral (closed symbols) and trioctahedral (open symbols) 2:1 layer silicates from Kinsey et al. (1985) (triangles) and Woessner (1989) (squares) are included for comparison. (Note: the trioctahedral mica ephesite plots on the dioctahedral mica trend. See discussion in Woessner, 1989.)

more symmetrical and would be expected as the $^{[4]}$Al/$^{[4]}$(Al + Si) ratio approaches 1.

We conclude that the integrated intensities of the peaks do not accurately reflect the amounts of $^{[4]}$Al and $^{[6]}$Al present. Woessner (1989) obtained comparable results for four trioctahedral clays with $^{[4]}$Al/($^{[4]}$Al + $^{[6]}$Al) ratios $\geq$0.5, but for several dioctahedral micas and clays in which $^{[6]}$Al > $^{[4]}$Al, Kinsey et al. (1985) and Woessner (1989) obtained excellent correlation between the results for ^{27}Al NMR spectroscopy and chemical analysis for samples with $^{[4]}$Al/($^{[4]}$Al + $^{[6]}$Al) ratios below ~0.4 (Fig. 7). Thus it appears if the amount of $^{[6]}$Al is greater than that of $^{[4]}$Al, analysis of ^{27}Al spectra can yield reasonably accurate $^{[4]}$Al/($^{[4]}$Al + $^{[6]}$Al) ratios, but when $^{[4]}$Al exceeds $^{[6]}$Al, the ^{27}Al spectra overestimate this ratio. Further work is needed to determine the solution to this difficulty.

The variation in the ^{29}Si chemical shifts and ^{27}Al peak maxima of $^{[4]}$Al are somewhat different from those of previous studies of 2:1 layer silicates (Kinsey et al., 1985; Weiss et al., 1987). For ^{29}Si, Weiss et al. (1987) observed deshielding of the peak for Q^3(0Al) Si sites with increasing $^{[4]}$Al/$^{[4]}$(Al + Si) ratio (Fig. 8), increasing tetrahedral rotation, substitutions that replace $^{[6]}$Mg (in trioctahedral) or $^{[6]}$Al (in dioctahedral), and the resulting increased negative layer charge. The ^{29}Si chemical shifts for the synthetic magnesium aluminum phlogopite samples vary much less, with those for the Q^3(0Al) site increasing ~1 ppm from X_{east} = 0.00–0.92 (Fig. 8) and those for the other Q^3(nAl) sites ranging nonsystematically within a range of 1 ppm. Correlations of chemical shift with $^{[6]}$Al content and tetrahedral rotation angle yielded similar results.

We believe the small variations in ^{29}Si chemical shift result from the counteracting effects of the $^{[4]}$(AlSi$_{-1}$) and $^{[6]}$(AlMg$_{-1}$) substitutions in the synthetic micas. The $^{[4]}$(AlSi$_{-1}$) substitution causes deshielding at ^{29}Si in Q^3 sites (e.g., Weiss et al. 1987). On the other hand, we would expect the $^{[6]}$(AlMg$_{-1}$) substitution to cause shielding at ^{29}Si because the electronegativity of Al is greater than that of Mg (1.6 vs. 1.38; see Smith et al., 1983 for a discussion of electronegativity and bond-strength effects).

The ^{27}Al peak maxima of $^{[4]}$Al in our spectra also become more positive with increasing $^{[4]}$Al/$^{[4]}$(Al + Si) (Fig. 9). The observed trend is consistent with the results of Woessner (1989) but is ~2 ppm more negative than for the trioctahedral samples of Kinsey et al. (1985). The data plotted are peak maxima, not isotopic chemical shifts, and are uncorrected for second-order quadrupole effects. Thus, smaller $^{[4]}$Al quadrupole coupling constants for the samples from Kinsey et al. (1985) could explain the observed discrepancies between the data sets.

Modeling of the ^{29}Si NMR spectra and $^{[4]}$Al-Si distribution

Computational methods

We have used computer modeling techniques to simulate the ^{29}Si NMR spectra of the synthetic magnesium aluminum phlogopite samples and to test the validity of various possible Al-Si distribution schemes. Four models were tested: random distribution, avoidance of Al-O-Al linkages only, homogeneous dispersion of charges, and long-range ordered distribution. In the computer algorithm used, Al and Si are systematically placed on sites in a hexagonal array that contains 10000 tetrahedral sites and 5000 hexagonal rings. Cyclic boundary conditions are imposed along the edges of the array. The only input data

are the $^{[4]}Al/^{[4]}(Al + Si)$ ratios determined from the microprobe analyses. The Al and Si atoms are placed in the array using the different constraints imposed by each model, and after the sheet is completely filled, the fractions of the $Q^3(nAl)$ sites are counted. The ability of a model to reproduce accurately the ^{29}Si spectra is assessed using the residual error (R) defined as (Herrero et al., 1987)

$$R = \sum_{n=0}^{3} |I_n^{obs} - I_n^{calc}| \quad (4)$$

where the I_n's are the observed and calculated intensities of the $Q^3(nAl)$ peaks. Briefly, the four models used are as follows.

1. Random distribution (RD): Randomly selected Al and Si are sequentially placed on sites in the array. Al and Si are randomly chosen using a random number generator and the observed $^{[4]}Al/^{[4]}(Al + Si)$ ratios (y). The ability of the RD program to model accurately a random Al-Si distribution can be checked by comparing the calculated $Q^3(0Al)$, $Q^3(1Al)$, $Q^3(2Al)$, and $Q^3(3Al)$ intensities to their statistical probabilities, which are $(1 - y)^3$, $3(1 - y)^2y$, $3(1 - y)y^2$, and y^3, respectively. The peak intensities from the computer model are within $\pm 1\%$ of the statistical probabilities for all y. The calculated intensities from the RD program are used for the comparison with the observed peak intensities.

2. Al-O-Al avoidance (AA): Randomly selected Al or Si is sequentially placed on the sites in the array. When Al is placed on an empty site, the NNN sites are immediately filled with Si, eliminating the possibility of adjacent Al tetrahedra. The probability of Al occupying a site increases nonlinearly with increasing $^{[4]}Al$ content to a maximum of 1.0 at $y = 0.5$ and was determined by trial and error for each y, based on the $^{[4]}Al$ content produced by the computer model. The calculated peak intensities from the AA program can be checked against the statistically determined $Q^3(0Al)$, $Q^3(1Al)$, $Q^3(2Al)$, and $Q^3(3Al)$ intensities, which are s^3, $3s^2a$, $3sa^2$, and a^3, where $a = y/(1 - y)$ and $s = 1 - a$ (Herrero et al., 1985a). For $y < 0.33$, the calculated peak intensities from the computer model are within $\pm 2\%$ of the statistical probabilities calculated from the above expressions. For $y > 0.33$, the calculated peak intensities are within $\pm 4\%$ for $Q^3(1Al)$, $\pm 1\%$ for $Q^3(3Al)$, and $\pm 8\%$ for $Q^3(0Al)$ and $Q^3(2Al)$ of the statistical probabilities. The intensities calculated from the AA program are used for the comparison with the observed peak intensities.

3. Homogeneous dispersion of charges (HDC): This model was proposed by Herrero et al. (1985a) and has been applied to 2:1 layer silicates with $^{[4]}Al/^{[4]}(Al + Si)$ ratios between $0.12 \leq y \leq 0.29$ (Herrero et al., 1985a, 1985b) and $y = 0.43$ (Herrero et al., 1987). A brief summary of the model is presented here, and a complete discussion is available in the preceding references. In this model, in addition to the restriction of Al-O-Al avoidance, the Al is distributed as evenly as possible among the rings in the sheet. For instance, a mica with a $^{[4]}Al/^{[4]}(Al + Si)$ ratio of 0.25 has 1 Al per four tetrahedral sites, which corresponds to an average of 1.5 Al in the six sites of a hexagonal ring of tetrahedra. For this composition, the tetrahedral sheet has an equal number of rings containing 1 and 2 Al and no rings with 0 or 3 Al. A mica with a $^{[4]}Al/^{[4]}(Al + Si)$ ratio of 0.40 has 1.6 Al per four tetrahedral sites and an average of 2.4 Al per six ring sites. For this composition, the tetrahedral sheet contains 60% rings with 2 Al, 40% rings with 3 Al, and no rings with 0 or 1 Al.

Rings that contain 0, 1, or 3 Al are symmetrically nonunique and interchangeable. However, rings containing 2 Al can have a para configuration (2P), in which Al sites are separated by 2 Si sites, or a meta configuration (2M), in which Al sites are separated by 1 and 3 Si sites. The ratio of 2M/2P rings is used as an independent variable in the model. In the program, Al and Si are placed in the sheet ring by ring according to the probabilities of the different ring types (1 or 2 Al per ring for $0.24 \leq y < 0.33$, 2 or 3 Al per ring for $0.33 < y \leq 0.50$) and a fixed ratio of 2M/2P. A range of 2M/2P ratios was tried for each $^{[4]}Al$ content. The calculated peak intensities for the mica with $X_{east} = 0.70$ are plotted as a function of the 2M/2P ratio in Figure 10. The residual error R is a minimum when the calculated intensities are equal to the observed intensities, at a 2M/2P ratio of ~2 for this mica (Fig. 10). The results for the HDC model in Table 7 produced the minimum R for each composition.

The ^{29}Si NMR spectra from Herrero et al. (1987) were modeled using our program for comparison, and we reproduced their results for the HDC model satisfactorily. For their vermiculite sample with $y = 0.28$, our HDC program produces a minimum $R = 6.7$ with a 2M/2P ratio of 2.3 compared with $R = 3.8$ and a 2M/2P of 2 from their HDC program. For their synthetic mica with $y = 0.43$, our HDC program produces a minimum $R = 0.8$ with a 2M/2P ratio of 0.8 compared with $R = 0.6$ and a 2M/2P of 1 from their HDC program.

4. Ordered sheet (ORD): In this model, alternating sites are filled with only Si and then the remaining sites are randomly filled with Al or Si, with the probability $2y$ that Al will occupy the site. This model produces long-range order in the tetrahedral sheet, complies with Al-O-Al avoidance, and allows only 2 Al rings with the meta configuration. The Al-Si distribution is analogous to a margarite-type tetrahedral sheet.

Results

The residual errors for the different Al-Si distribution models clearly show that the HDC model reproduces the observed peak intensities of the ^{29}Si NMR spectra of the synthetic magnesium aluminum phlogopite samples more accurately than the other models (Table 7, Fig. 11), in agreement with the results of Herrero et al. (1985a, 1985b, 1987). The RD model produces high residual errors, clearly indicating that Al-O-Al linkages are minimized in the tetrahedral sheets of our samples. The avoidance of Al-O-Al linkages is the predominant factor limiting the distribution of Al and Si, which is indicated by the signifi-

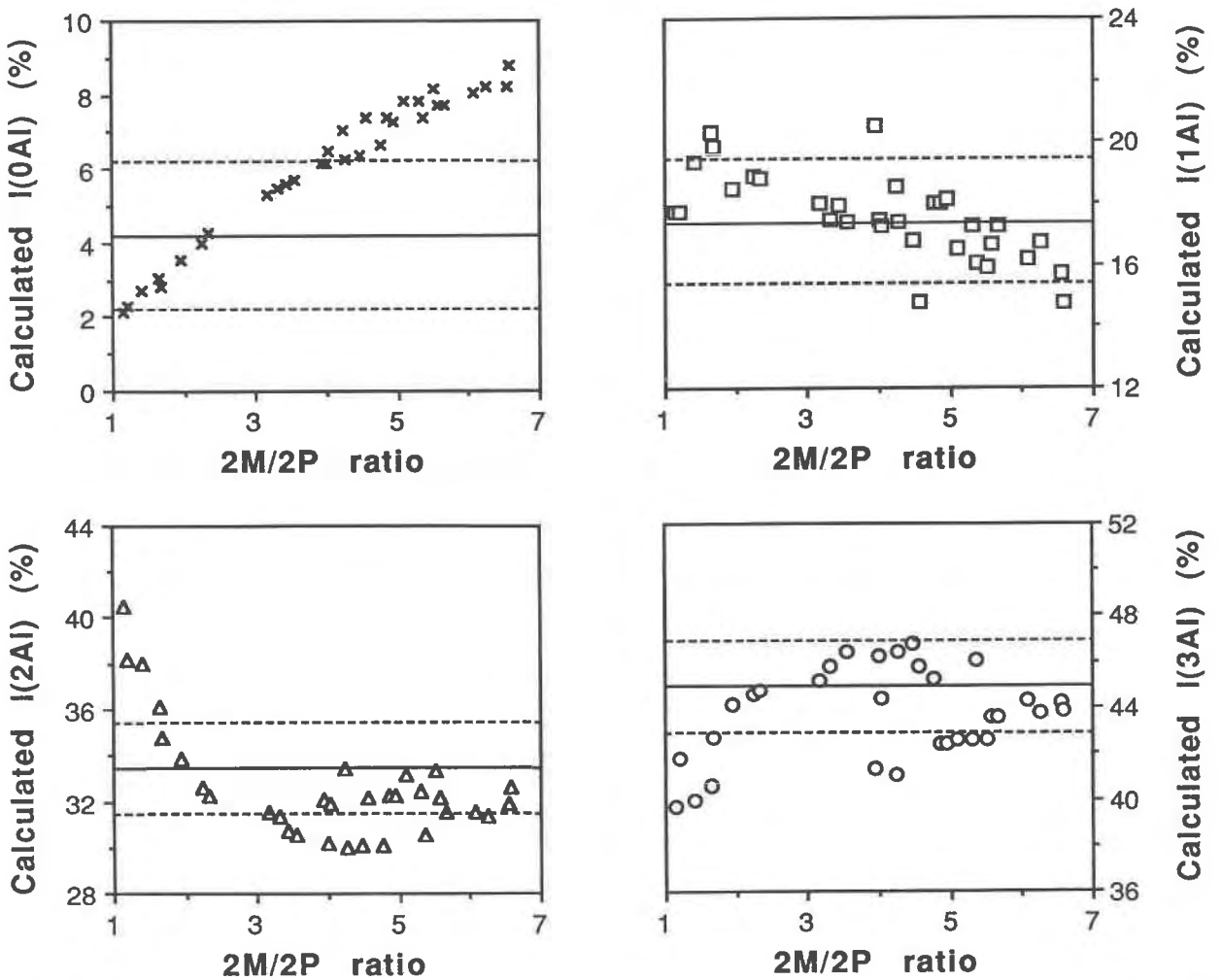

Fig. 10. Calculated relative peak intensities of the $Q^3(n\text{Al})$ components from the HDC model vs. the 2M/2P ratio for the synthetic magnesium aluminum phlogopite with $X_{east} = 0.70$. The horizontal line represents the observed relative intensity of that peak in the ^{29}Si NMR spectrum, and the dashed lines represent the uncertainty in each peak intensity.

cantly lower residual errors for the AA model and the correlation between observed and calculated peak intensities, especially at $^{[4]}Al/^{[4]}(Al + Si)$ ratios above 0.3 (Fig. 6). The further constraint of homogeneous dispersion of Al throughout the sheet improves on the AA model. The residual errors for the long-range ordered model (ORD) are high at low $^{[4]}$Al contents, where short-range ordering from Al-O-Al avoidance predominates, and decrease with increasing $^{[4]}$Al content as the sheets become increasingly long-range ordered with increasing $^{[4]}$Al content, resulting in margarite-like domains of strictly alternating Al and Si tetrahedra (e.g., Fig. 6b of Herrero et al., 1987).

We are unable to reproduce the observed peak intensities using the HDC model for the mica with $X_{east} = 0.92$ ($y = 0.47$). Low residual errors are obtained only if we assume $y = 0.44$, the calculated $^{[4]}Al/^{[4]}(Al + Si)$ ratio from the ^{29}Si NMR spectra, because the calculated intensity of the Q^3(3Al) component increases sharply with increasing $^{[4]}$Al, producing high (>10%) residual errors. This disparity is discussed below.

For the HDC model of the mica with $X_{east} = 0.32$ ($y = 0.32$), we could not locate the optimum 2M/2P ratio to produce a minimum residual error of less than 8% because the HDC program would not make sheets with 2M/2P ratios higher than 4.5 for this $^{[4]}$Al content. Nonetheless, the HDC model reproduces the observed peak intensities more accurately and produces a lower residual error than any of the other models. No modeling results for 2:1 layer silicates with $^{[4]}Al/^{[4]}(Al + Si)$ ratios near 0.33, which would contain only 2 Al rings in the HDC model, are available in the literature for comparison.

Discussion

The 2M/2P ratios that produce the best fits for the spectra in this study are higher than those found by Herrero et al. (1987) for micas with comparable $^{[4]}$Al contents.

TABLE 7. Calculated peak intensities of the Q³(*n*Al) Si sites from different Al-Si distribution models

X_{east}	Model*	0Al	1Al	2Al	3Al	R**	2M/2P	X_{east}	Model	0Al	1Al	2Al	3Al	R**	2M/2P
0.00	RD	44.4	41.3	13.0	1.3	44.0		0.56	RD	25.7	44.3	25.0	5.1	63.6	
	AA	32.7	45.0	19.8	2.5	23.3			AA	13.3	29.9	38.0	18.8	10.9	
	ORD	43.8	26.1	23.1	7.0	61.3			ORD	23.0	12.6	33.4	31.0	41.6	
	HDC	24.3	57.0	17.8	0.9	3.5	2.2		HDC	7.9	28.7	39.2	24.2	3.1	4.0
	OBS	23.7	56.7	19.6	0.0	2.4			OBS	8.9	29.2	37.6	24.2	2.9	
0.13	RD	41.4	42.0	15.0	1.7	43.1		0.70	RD	20.5	42.5	30.1	7.0	82.8	
	AA	28.3	44.0	23.8	3.9	21.7			AA	10.8	16.6	36.0	36.6	18.1	
	ORD	40.5	24.4	25.8	9.3	60.7			ORD	15.4	6.5	30.4	47.7	27.9	
	HDC	19.2	56.0	22.8	1.9	2.5	2.5		HDC	4.0	18.9	32.6	44.5	3.0	2.2
	OBS	19.8	54.8	22.9	2.5	3.2			OBS	4.2	17.4	33.5	44.9	4.0	
0.24	RD	34.5	44.0	19.0	2.6	44.3		0.80	RD	18.8	41.7	32.0	7.6	91.9	
	AA	19.6	40.2	31.5	8.6	22.9			AA	9.4	12.4	34.4	43.8	19.3	
	ORD	33.1	20.2	31.1	15.4	63.8			ORD	12.5	4.4	27.4	55.7	17.4	
	HDC	12.9	50.1	32.6	4.4	1.3	4.0		HDC	6.2	13.3	28.7	51.8	3.4	4.4
	OBS	12.3	50.0	33.2	4.5	3.2			OBS	6.0	12.0	28.5	53.5	5.1	
0.32	RD	30.7	44.5	21.2	3.6	47.3		0.92†	RD	17.3	41.8	32.4	8.6	91.4	
	AA	16.2	36.8	34.9	12.1	20.2			AA	9.1	9.9	31.1	49.8	24.3	
	ORD	29.5	17.7	33.3	19.5	61.5			ORD	10.9	3.4	24.8	61.0	33.0	
	HDC	8.3	44.5	41.2	5.9	8.0	4.4		HDC	2.8	14.8	27.4	55.0	5.6	2.0
	OBS	10.5	41.1	40.7	7.7	3.6			OBS	1.0	17.6	27.1	54.3	4.8	
0.45	RD	27.0	44.6	24.0	4.4	63.7									
	AA	14.3	31.0	38.8	15.8	13.2									
	ORD	24.4	14.0	34.5	27.1	55.1									
	HDC	8.8	33.7	41.8	15.7	5.6	4.1								
	OBS	7.8	32.0	44.1	16.2	3.2									

Note: Calculated probabilities are normalized to 100%.

* Model abbreviations: RD = random distribution, AA = Al-O-Al avoidance, ORD = long-range ordered distribution, HDC = homogeneous dispersion of charges, OBS = observed intensities.

** Residual error of model (defined in text). The values listed for OBS are the propagated uncertainties of the peak intensities listed in Table 6.

† Model results for this sample were based on the [4]Al/[4](Al + Si) ratio of 0.44 (see discussion in text).

For example, the observed peak intensities for Q³(*n*Al) sites with $n = 0$, 1, 2, and 3 for our mica with $X_{east} = 0.13$ ($y = 0.27$) are 19.8, 54.8, 22.9, and 2.5, respectively (Table 6), whereas those of a vermiculite with $y = 0.28$ from Herrero et al. (1987) are 15.5, 54.0, 30.5, and 0.0, respectively. The calculated 2M/2P ratio for our mica is 2.5 and for their mica is ~2. Similarly, the observed intensities for our mica with $X_{east} = 0.80$ ($y = 0.44$) are 6.0, 12.0, 28.5, and 53.5, whereas those of a synthetic trioctahedral clay with $y = 0.43$ from Herrero et al. (1987) are 1.0, 13.8, 38.0, and 47.2. The calculated 2M/2P ratio for our mica is 4.4 and for their mica is ~1. In general, increasing the 2M/2P ratio increases the calculated intensities of sites with 0 and 3 Al relative to those of sites with 1 and 2 Al (Fig. 10) and implies an increase in Al-Si order. This result suggests that for a given [4]Al content the tetrahedral sheets of the synthetic magnesium aluminum phlogopite samples may be more ordered than a distribution solely limited by Al avoidance and homogeneous dispersion of charges. It does not imply, however, that the sheets are long-range ordered. The residual errors for the ordered model are significantly higher than those for the HDC model, even at high [4]Al contents (Table 7, Fig. 11). Thus, although ordering in the tetrahedral sheet increases with increasing [4]Al content, Al and Si are distributed almost as randomly as the constraint of HDC permits.

The microprobe analysis of the mica with $X_{east} = 0.92$ yields a [4]Al content of $y = 0.47$, whereas analysis of the ²⁹Si NMR spectrum yields $y = 0.44$. This may imply that strict Al-O-Al avoidance is not valid for this mica. It is clear from Figure 11 that a completely random distribution of Al and Si also does not reproduce the observed ²⁹Si NMR spectra, and the similarity of the microprobe and ²⁹Si NMR values indicates a low concentration of Al-

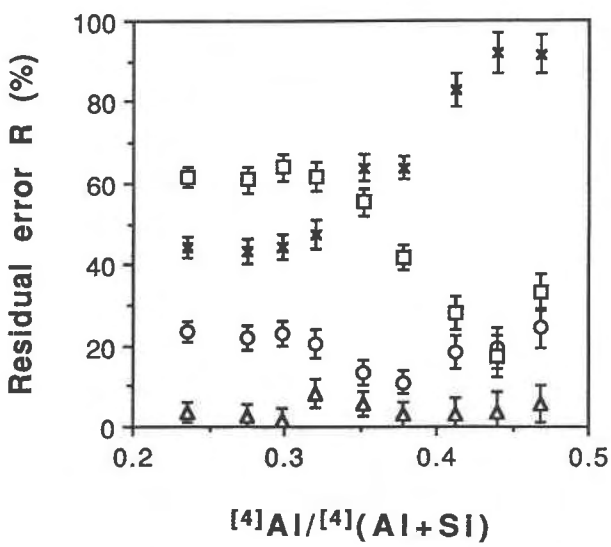

Fig. 11. Residual errors for the RD (crosses), AA (circles), HDC (triangles), and ORD (squares) models vs. the [4]Al/[4](Al + Si) ratio calculated from microprobe analysis. Brackets represent the propagated uncertainties in the observed peak intensities.

O-Al linkages. The fraction of Al-O-Al linkages can be calculated from the expression (Barron et al., 1985)

$$\text{density(Al-O-Al)} = \frac{3}{2} y_{pr} - \frac{3}{2}(1 - y_{pr})\frac{Al}{Si} \qquad (5)$$

where y_{pr} is the [4]Al content measured by microprobe analysis (0.468) and Al/Si (0.792) is calculated from the observed peak intensities and Equation 3. For the mica with $y = 0.47$, the fraction of Al-O-Al linkages is 0.070. To simulate a tetrahedral sheet with an Al-Si distribution governed primarily by HDC with some Al-O-Al linkages, we modified the HDC model by randomly placing 500 Al not surrounded by NNN Si in the tetrahedral sheet and then placing the remaining Al and Si into the sheet using the HDC program as described above. The resulting tetrahedral sheet contains several Al-O-Al linkages, in part indicated by the presence of rings with more than 3 Al (~3%). The calculated intensities of the $Q^3(n\text{Al})$ components of the simulated spectrum using this modified HDC program are 2.0, 15.2, 26.4, and 56.4 for $n = 0$, 1, 2, and 3, respectively, and the residual error is 6.4. We conclude that although the small discrepancy between the [4]Al content of this mica from microprobe analysis and ^{29}Si NMR can arise from Al-O-Al linkages in the tetrahedral sheet, the Al-Si distribution of all the synthetic magnesium aluminum phlogopite samples, including that with $X_{east} = 0.92$, is primarily governed by the avoidance of Al-O-Al linkages.

We have not considered the Mg-Al distribution in the octahedral sites, and the analytical techniques used in this study provide little information. The smaller Al cation should be disordered on the two M2 sites, which are smaller on average than the M1 site, based on structure refinements of natural micas (Bailey, 1984). The HDC model used to model the Al-Si distribution does not include the electrostatic interactions between tetrahedral and octahedral sheets, which may also control the distribution of octahedral and tetrahedral cations. Electrostatic interactions of the hexagonal (Al-Si) rings with the interlayer cations and between adjacent tetrahedral sheets in contiguous 2:1 layers have been shown to contribute to the observed Al-Si distributions (Herrero et al., 1986).

Conclusions

The increasing [6,4]Al content of the synthetic magnesium aluminum phlogopite samples is described by the Tschermak's substitution ([6]Al,[4]Al)([6]Mg,[4]Si)$_{-1}$, and the range of solid solution appears to extend across the phlogopite-eastonite join. The unit-cell volume of magnesium aluminum phlogopite decreases linearly with increasing [6,4]Al content and is linked to the decreasing lateral dimensions of the octahedral sheet. The increased misfit with the larger tetrahedral sheets is compensated by increased counterrotation of the tetrahedra, which reduces the size of the interlayer cavity and increases the structural distortions in the mica. The Al-Si distributions in the tetrahedral sheets of all the magnesium aluminum phlogopite samples are short-range ordered, best described by the homogeneous dispersion of charges in which [4]Al is distributed randomly and evenly throughout the sheet and no Al-O-Al linkages are permitted.

Acknowledgments

The gel synthesis, XRD, computer modeling, and electron microprobe analysis work were supported by the U.S. Department of Energy (grant DE-FG02-85ER-13437). The experimental petrology and the electron microprobe analysis work at the University of Edinburgh were supported by NERC. The NMR spectroscopy work at the University of Illinois was supported by NSF (grant EAR-8706729). We are indebted to the following people: at Princeton University, S. Swapp for assistance with electron microprobe analysis and X-ray diffraction and the use of LSMODES and C. Bennett, who designed and built the TGA furnace; at the University of Edinburgh, M. Welch, A. Pawley, and S. Elphick in the experimental petrology lab for advice and discussion, P. Hill for assistance with electron microprobe analysis, and D. James for the XRF analyses of the gels; at the University of Illinois, B. Montez for NMR data acquisition and B. Phillips for curve fitting the NMR spectra. We thank B.L. Sherrif, D. Spearing, and J. Stebbins for their constructive and expeditious reviews.

References cited

Appleman, D.E., and Evans, H.T. (1973) Job 9214: Indexing and least-squares refinement of powder diffraction data. U.S. National Technical Information Service, Document PB 216 88.

Bailey, S.W. (1984) Crystal chemistry of the true micas. In Mineralogical Society of America Reviews in Mineralogy, 13, 13–57.

Barron, P.F., Slade, P., and Frost, R.L. (1985) Ordering of aluminum in tetrahedral sites in mixed-layer 2:1 phyllosilicates by solid-state high-resolution NMR. Journal of Physical Chemistry, 89, 3880–3885.

Brinker, C.J., Bunker, B.C., Tallant, D.R., Ward, K.J., and Kirkpatrick, R.J. (1988) Structure of sol-gel-derived inorganic polymers: Silicates and borates. In M. Zelden, K.J. Wynne, and H.R. Allcock, Eds., Inorganic and organometallic polymers, p. 314–332. American Chemical Society, Washington, DC.

Bryan, W.B., Finger, L.W., and Chayes, F. (1969) Estimating proportions in petrographic mixing equations by least-squares approximation. Science, 163, 926–927.

Circone, S., and Navrotsky, A. (1990) Thermochemistry of the phlogopite-eastonite join. Eos, 71, 1648–1649.

Clemens, J.D., Circone, S., Navrotsky, A., McMillan, P.F., Smith, B.K., and Wall, V.J. (1987) Phlogopite: High temperature solution calorimetry, thermodynamic properties, Al-Si and stacking disorder, and phase equilibria. Geochimica et Cosmochimica Acta, 51, 2569–2578.

Crowley, M.S., and Roy, R. (1964) Crystalline solubility in the muscovite and phlogopite groups. American Mineralogist, 49, 348–362.

Dupree, R., Lewis, M.H., and Smith, M.E. (1988) Structural characterization of ceramic phases with high-resolution ^{27}Al NMR. Journal of Applied Crystallography, 21, 109–116.

Guidotti, C.V. (1984) Micas in metamorphic rocks. In Mineralogical Society of America Reviews in Mineralogy, 13, 357–467.

Hamilton, D.L., and Henderson, C.M.B. (1968) The preparation of silicate compositions by a gelling method. Mineralogical Magazine, 36, 832–838.

Herrero, C.P., Sanz, J., and Serratosa, J.M. (1985a) Si, Al distribution in micas: Analysis by high-resolution ^{29}Si NMR spectroscopy. Journal of Physics C: Solid State Physics, 18, 13–22.

——— (1985b) Tetrahedral cation ordering in layer silicates by ^{29}Si NMR spectroscopy. Solid State Communications, 53, 151–154.

——— (1986) The electrostatic energy of micas as a function of Si,Al tetrahedral ordering. Journal of Physics C: Solid State Physics, 19, 4169–4181.

Herrero, C.P., Gregorkiewitz, M., Sanz, J., and Serratosa, J.M. (1987) ^{29}Si MAS-NMR spectroscopy of mica-type silicates: Observed and predicted distribution of tetrahedral Al-Si. Physics and Chemistry of Minerals, 15, 84–90.

Hewitt, D.A., and Wones, D.R. (1975) Physical properties of some synthetic Fe-Mg-Al trioctahedral biotites. American Mineralogist, 60, 854–862.

——— (1984) Experimental phase relations of the micas. In Mineralogical Society of American Reviews in Mineralogy, 13, 201–256.

Kinsey, R.A., Kirkpatrick, R.J., Hower, J., Smith K.A., and Oldfield, E. (1985) High resolution aluminum-27 and silicon-29 nuclear magnetic resonance spectroscopic study of layer silicates, including clay minerals. American Mineralogist, 70, 536–548.

Lippmaa, E., Mägi, M., Samoson, A., Engelhardt, G., and Grimmer, A.-R. (1980) Structural studies of silicates by solid-state high-resolution ^{29}Si NMR. Journal of the American Chemical Society, 102, 4889–4893.

Lipsicas, M., Raythatha, R.H., Pinnavaia, T.J., Johnson, I.D., Giese, R.F., Costanzo, P.M., and Robert, J.-L. (1984) Silicon and aluminium site distributions in 2:1 layered silicate clays. Nature, 309, 604–607.

Livi, K.J.T., and Veblen, D.R. (1987) "Eastonite" from Easton, Pennsylvania: A mixture of phlogopite and a new form of serpentine. American Mineralogist, 72, 113–125.

Loewenstein, W. (1954) The distribution of aluminum in the tetrahedra of silicates and aluminates. American Mineralogist, 39, 92–96.

Mägi, M., Lippmaa, E., Samoson, A., Engelhardt, G., and Grimmer, A.-R. (1984) Solid-state high-resolution silicon-29 chemical shifts in silicates. Journal of Physical Chemistry, 88, 1518–1522.

Müller, D., Gessner, W., Behrens, H.-J., and Scheler, G. (1981) Determination of the aluminium coordination in aluminium-oxygen compounds by solid-state high-resolution ^{27}Al NMR. Chemical Physics Letters, 79, 59–62.

Press, W.H., Flannery, B.P., Teukolsky, S.A., and Vetterling, W.T. (1986) Numerical recipes, the art of scientific computing, 818 p. Cambridge University Press, Cambridge, New York.

Radoslovich, E.W. (1961) Surface symmetry and cell dimensions of layer lattice silicates. Nature, 191, 67–68.

Radoslovich, E.W., and Norrish, K. (1962) The cell dimensions and symmetry of layer-lattice silicates. American Mineralogist, 47, 599–616.

Robert, J.-L. (1976) Phlogopite solid solutions in the system K_2O-MgO-Al_2O_3-SiO_2-H_2O. Chemical Geology, 17, 195–212.

Sanz, J., and Serratosa, J.M. (1984) ^{29}Si and ^{27}Al high-resolution MAS-NMR spectra of phyllosilicates. Journal of the American Chemical Society, 106, 4790–4793.

Shannon, R.D., and Prewitt, C.T. (1969) Effective ionic radii in oxides and fluorides. Acta Crystallographica, B25, 925–946.

Smith, K.A., Kirkpatrick, R.J., Oldfield, E., and Henderson, D.M. (1983) High-resolution silicon-29 nuclear magnetic resonance spectroscopic study of rock-forming silicates. American Mineralogist, 68, 1206–1215.

Speer, J.A. (1984) Micas in igneous rocks. In Mineralogical Society of America Reviews in Mineralogy, 13, 299–356.

Turner, G.L., Smith, K.A., Kirkpatrick, R.J., and Oldfield, E. (1986) Boron-11 nuclear magnetic resonance spectroscopic study of borate and borosilicate minerals and a borosilicate glass. Journal of Magnetic Resonance, 67, 544–550.

Vedder, W., and Wilkins, R.W.T. (1969) Dehydroxylation and rehydroxylation, oxidation and reduction of micas. American Mineralogist, 54, 482–507.

Weiss, C.A., Altaner, S.P., and Kirkpatrick, R.J. (1987) High-resolution ^{29}Si NMR spectroscopy of 2:1 layer silicates: Correlations among chemical shift, structural distortions, chemical variations. American Mineralogist, 72, 935–942.

Woessner, D.E. (1989) Characterization of clay minerals by ^{27}Al nuclear magnetic resonance spectroscopy. American Mineralogist, 74, 203–215.

Yoder, H.S., and Eugster, H.P. (1954) Phlogopite synthesis and stability range. Geochimica et Cosmochimica Acta, 6, 157–185.

Manuscript received November 5, 1990
Manuscript accepted May 21, 1991